processes

MDPI

Article

Modeling and Simulation of the Induction Hardening Process: Evaluation of Gear Deformations and Parameter Optimization

Pedro Maranhão Pinheiro [1], José Urbano Junio [2], Lídice Aparecida Pereira Gonçalves [2], José Ângelo Peixoto da Costa [1,2], Alvaro Antonio Villa Ochoa [1,2,*], Kleber Gonçalves Bezerra Alves [1], Gustavo de Novaes Pires Leite [1,2] and Paula Suemy Arruda Michima [1]

[1] Department of Mechanical Engineering, Federal University of Pernambuco, Cidade Universitaria, 1235, Recife 50670-901, Brazil; pedro.pinheiro@ufpe.br (P.M.P.); angelocosta@recife.ifpe.edu.br (J.Â.P.d.C.); kleber.gbalves@ufpe.br (K.G.B.A.); gustavonovaes@recife.ifpe.edu.br (G.d.N.P.L.)

[2] Department of Higher Education Courses (DACS), Federal Institute of Education, Science and Technology of Pernambuco, Av. Prof. Luiz Freire, 500, Recife 50740-545, Brazil; josejunio@recife.ifpe.edu.br (J.U.J.); lidicegoncalves@recife.ifpe.edu.br (L.A.P.G.)

* Correspondence: ochoaalvaro@recife.ifpe.edu.br; Tel.: +55-81-99976-4266

Abstract: This study aimed to analyze and optimize the thermal induction hardening process applied to toothed transmission gears, focusing on thermal aspects, structural deformation, and topology optimization, while exploring the feasibility of various materials and operating conditions. The research simulated thermal and deformation behavior using a computer model, comparing results with experimental data through the Ansys® platform 2022 R1. The methodology encompassed thermal and deformation analyses, topology optimization to identify removable regions without compromising part integrity, and a sensitivity study to evaluate the different materials and operating conditions. This study validates the precision of computational models in predicting thermal and deformation behavior in toothed gears under thermal induction hardening, introducing topology optimizations and alternative materials, and providing novel perspectives for the more efficient and cost-effective manufacturing of these components. Comparative thermal analysis revealed a maximum relative error of less than 6% between temperatures from the computer model and experimental results, while deformation comparisons exhibited a maximum relative error of less than 7%, affirming the simulation model's accuracy in predicting and managing deformations within acceptable thresholds. Topology optimization successfully pinpointed removable regions without compromising structural integrity, enabling the production of lighter and more economical devices. Future endeavors should concentrate on additional tests to verify the feasibility of reducing power and cooling temperature without compromising product specifications. Furthermore, it is advisable to explore alternative materials and apply the developed methodology in diverse industrial settings to generalize the findings and amplify the impact of the proposed optimizations.

Keywords: heat treatment; numerical analysis; induction; distortions; topology optimization

Citation: Pinheiro, P.M.; Junio, J.U.; Gonçalves, L.A.P.; da Costa, J.Â.P.; Ochoa, A.A.V.; Alves, K.G.B.; Leite, G.d.N.P.; Michima, P.S.A. Modeling and Simulation of the Induction Hardening Process: Evaluation of Gear Deformations and Parameter Optimization. *Processes* **2024**, *12*, 1428. https://doi.org/10.3390/pr12071428

Academic Editors: Vladimir D. Stevanovic and Ritunesh Kumar

Received: 7 June 2024
Revised: 30 June 2024
Accepted: 6 July 2024
Published: 9 July 2024

1. Introduction

Gears, essential mechanical components for transmitting motion, find applications across various industries such as automotive, aeronautics, and renewable energy [1–3]. In the motorcycle sector, toothed gears primarily transmit the motion to the wheels from the combustion cycle of fossil fuel and/or biofuel engines [4,5].

The gear manufacturing process comprises a range of process flows [6], selecting the most suitable flow contingent upon material, product geometry, tolerances, and appearance requirements. Among these, heat treatment stands out as the most critical manufacturing step due to its complexity [7–11].

Induction hardening, a widely employed technique in the automotive industry, enhances the mechanical properties of components like gears and engine parts [12]. This

process involves rapid electromagnetic induction heating followed by swift cooling, resulting in a hardened surface and a more resilient core. Therefore, in the case of gears, the process is a sequence of heating and cooling cycles to alter the steel's metallographic structure and mechanical properties. Modeling and simulating this process are pivotal for optimizing operational parameters, minimizing undesired deformations, and ensuring component quality and longevity [13]. Park et al. [13] developed a numerical model coupling thermal, mechanical, and metallurgical analysis to investigate the phase distribution and residual stresses under the induction heating process. However, the simulated results showed residual stresses higher than the experimentally measured value since the proposed model did not consider self-tempering during quenching. However, the estimates of deformations caused by thermal induction have not been evaluated.

The heat treatment cycle, involving heating and subsequent cooling, induces distortions due to temperature gradients. These distortions lead to dimensional variations in the product, necessitating adjustments in pre-heat treatment transformation operations to compensate for distortions or achieve final dimensions in post-heat treatment finishing processes, as evidenced in the literature [14]. Understanding these distortions during heat treatment is crucial for meeting final product specifications, reducing testing time, and defining manufacturing parameters in advance [15,16]. Sun et al. [15] developed a finite element model (FEM) to evaluate the stress–strain field, temperature field, and structural variations of the gear microstructure subjected to carburizing treatment. The model predicts gear deformations depending on the type of specific microstructure of the steel and only in the particular case of carburizing treatment.

Optimizing parameters and minimizing deformations are pivotal in induction hardening, particularly for precision components like gears [3,15]. Detailed modeling and simulation enable the fine-tuning of process parameters to achieve desired outcomes. Tyflopoulos et al. [17] utilized topological optimization tools to reduce the weight of automotive brake calipers, emphasizing the significance of design optimization in mechanically loaded components. While their focus was on additive manufacturing, the study's methods apply to hardening process optimization, where they achieved a weight reduction of over 40% and a 17% decrease in deformations.

Similarly, Borda et al. [18] and Lee et al. [19] concentrated on the topological optimization of vehicle supports, exploring different manufacturing methods and assessing component strength. Both studies employed ABAQUS software 2018 to validate optimizations, leading to substantial enhancements in the component strength and a weight reduction of approximately 40% and 15%, respectively. Armentani et al. [20] devised an optimization model to revamp engine mounts to diminish vibrations and enhance passenger comfort. Structural analysis played a crucial role in validating the fresh design, showcasing the practical application of optimization techniques to automotive components.

Huang et al. [21] explored the aerodynamic characteristics of a high-speed gearbox, investigating the effects of varying negative pressures and speeds on wind power loss. In contrast, their focus differed from the previously referred works. The simulation methodology for understanding operational variable impacts is relevant to studying gear deformations. Mitov et al. [22] utilized CFD modeling to analyze flow in gear pumps, underscoring the importance of simulation in comprehending complex phenomena in mechanical components.

Dziatkiewicz et al. [23] employed the response surface methodology and the desirability function to optimize the induction hardening parameters of rack bars. The integration of evolutionary algorithms, such as the genetic algorithm, effectively enhanced process quality under industrial conditions. In a parallel study, Garois et al. [24] developed a machine learning model to optimize the induction hardening process of C45 gears. The study encompassed two stages: initially utilizing machine learning techniques for modeling and validating the proposed approach's efficiency. The direct verification of the problem's results confirmed the effectiveness of the proposed approach, with 31 tests comprising

60 hardness measurement points each, showcasing the method's robustness in predicting process parameters from hardness data.

Numerous studies have investigated the modeling and simulation of induction hardening [24,25]. Jan and MacKenzie [26] proposed a computational model based on computational fluid mechanics (CFD) to calculate temperature profiles in automotive components during tempering. Their methodology aimed to optimize the tempering processes by managing residual thermal stresses that can induce distortions. Similarly, Saputro et al. [25] developed a specific numerical simulation for the induction hardening of spur gears in mechanical presses. The model addressed problems of insufficient hardening in the root areas and non-uniformity in the depth of hardening along the circumference of the teeth. The experimental validation of the model showed that adjustments to scanning speeds and air gaps can significantly improve hardening uniformity. Areitioaurtena et al. [27] conducted a study to predict the depth of the induced layer and hardness in 42CrMo4 billets during induction hardening, utilizing a semi-analytical model to reduce computational effort. The combination of finite element analysis for electromagnetic field calculations and analytical equations for thermal analysis yielded an efficient and accurate simulation, with less than a 4% difference between simulated and experimental results, validating the model's effectiveness and providing a 20% reduction in computational time. Min et al. [28] investigated the induction heating of a graphite crucible using COMSOL software 2021, establishing a correlation between the inductor current and crucible temperature while analyzing surface effects to determine the optimal heating frequency. The model's accuracy, with a relative error of less than 6%, underscored its effectiveness.

Leitner et al. [29] used thermo-metallurgical-mechanical simulations to evaluate the fatigue resistance of induction-treated steel components, emphasizing the integration of different manufacturing processes for a comprehensive fatigue resistance analysis. Fatigue test results revealed that induction hardening led to a 46% increase in fatigue strength amplitude compared to the initial base material. Notably, Barglik et al. [30] developed mathematical models to predict hardness and microstructure distributions in the transmission crown, which is crucial for understanding the impact of induction heating on material properties. The most relevant results showed the influence of the critical temperature and the properties of the investigated steel in determining the hardening temperature. The proposed mathematical model can be an effective tool for designing such processes; it makes it possible to predict hardness and microstructure distributions with a reasonable accuracy of about 20 HV. Artificial intelligence methods explored by Holmberg et al. [31] used Barkhausen noise (BN) for the non-destructive verification of induction hardening depth, resulting in a validated multivariate predictive model for evaluating hardening depths. Different Barkhausen noise parameters, such as RMSFWHM and MVSS (200 Hz, 20 Hz), show correlations with hardening depths up to 4.5 mm, indicating their potential for depth measurements. With the proposed method, it is possible to predict the hardening depth using principal components based on all or a reduced set of BN characteristics. However, the authors did not evaluate the estimates of deformations caused by thermal induction.

The experimental validation of numerical models is essential for ensuring simulation accuracy. In this context, various studies have produced data that allow numerical models to be verified as tools for simulating and optimizing manufacturing processes. Mitov et al. [22] validated a two-dimensional CFD model through experimental studies. Stević et al. [32] presented a comparative analysis of experimental and simulated results for an induction hardening system, demonstrating consistency in characteristic values from both qualitative and quantitative perspectives. Correa-Jullian et al. [33] evaluated various concentrations of polyethylene glycol (PAG) as a cooling medium and their impact on the dimensional distortions of an induction-hardened SAE 1050 steel shaft tip, revealing that a 10% PAG solution exhibited similar characteristics to a 5% solution but with more pronounced distortions exceeding dimensional tolerance limits.

This study aims to utilize simulation to quantify distortions occurring during treatment, evaluate the transmission crown attachment devices for potential mass reduction through topological optimization, and conduct a case study by varying process parameters to assess their influence on distortion and temperature values. Hence, it fills an existing gap in predicting structural deformation due to thermal induction, mainly in topographic optimization in toothed crowns, through computer simulation and validation in processes already applied in the automobile industry and evaluating alternative materials' viability. Based on this survey of the state of the art, this study brings the following contributions as innovation:

- Development and analysis of an optimization procedure for the thermal induction hardening process in toothed transmission gears focusing on thermal behavior, structural deformation, and, finally, topology optimization;
- Introduction of topology optimization in the thermal induction processes of toothed transmission gears to identify areas that can be removed without compromising the integrity of the part, resulting in the production of lighter and more economical components;
- Analysis of the efficiency of the thermal induction process in gears, highlighting advances in the understanding and control of this process and demonstrating improvements in manufacturing toothed transmission crowns with greater precision and lower cost.

2. Materials and Methods

This section presents the analysis of the induction hardening process of a motorcycle transmission crown. The methodological approach comprises seven stages: measurement of the part, hardening process, repetition of the measurement, 3D model development, thermal analysis, structural analysis, and optimization. Figure 1 is the flowchart of the implemented methodology's stages.

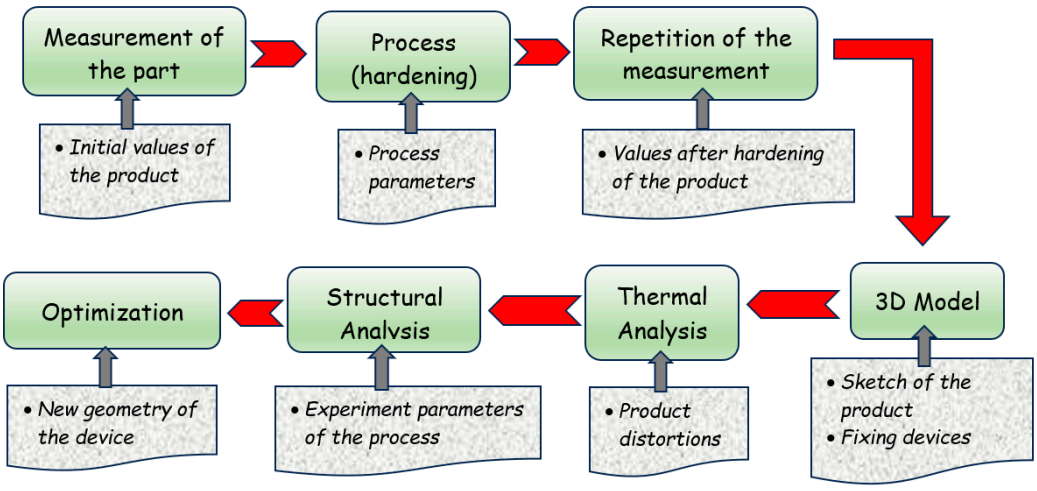

Figure 1. Flowchart of the methodology implemented.

The study begins with the initial measurements of the parts under production and experimental data collection. Next, the tempering process is applied to the manufactured parts, followed by a new measurement stage on the tempered components. The data from post-hardening measurements are then used to build the 3D model. The subsequent stages focus on modeling and computer simulation, utilizing thermal analysis (tempering process) and structural analysis (evaluating part distortions). The final stage of the implemented methodology involves topological optimization to assess the product's fastening device to reduce weight.

2.1. Experimental Analysis

This experimental analysis aims to collect the parameters needed to validate the numerical model of a transmission crown during its manufacturing process. The manufacturing process begins with the reception of the SAE 1045 carbon steel blank. This blank is then taken to the stamping phase, where relief cuts, fixing holes, and central and external holes are made. Since the stamping cannot meet the final tolerances, the central and external holes will undergo finishing processes. Next, the stamped part is sent to machining, where the outer and central holes are machined to their final dimensions, and the teeth are machined. The piece then undergoes heat treatment, specifically tempering through induction hardening, where it is heated via electromagnetic induction and cooled with water and additives. Afterward, the crown receives a surface treatment (zinc plating) to protect against oxidation. Finally, it is packaged and sent to the customer.

2.1.1. Product

A gearbox developed in the Brazilian motorcycle industry was selected. Table 1 shows the general specifications of the gearbox.

Table 1. The main dimensions of the transmission crown of this study.

Material	SAE 1045
Outside diameter	163 mm
Internal diameter	76 mm
Thickness	7.2 mm
Number of teeth	39
Chain	428

Due to the maker's project secrecy, other specifications, such as tenacity, elasticity, and their respective tolerances and tolerances, are omitted (company confidentiality). Figure 2 shows a general diagram of the part used.

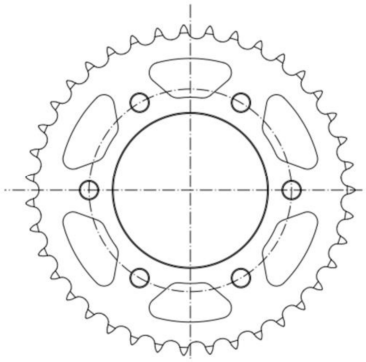

Material	SAE 1045
Outside diameter	163 mm
Internal Diameter	76 mm
Thickness	7.2 mm
Number of Teeth	39
Chain	428

Figure 2. Overview of the transmission crown studied.

2.1.2. Induction Hardening

The induction hardening process commences when the workpiece is introduced into the equipment. The utilized equipment features a rotating table with four stations solely dedicated to the hardening of carbon steel crowns for induction. The system is equipped with 125 kW of power and operates at a frequency of 30 Hz (Figure 3).

Figure 3. Induction hardening equipment.

The initial station is responsible for loading and unloading the equipment. In the process, the crown is positioned on a fixed base attached to a rotating table. Upon the initiation of the treatment cycle, the table rotates clockwise, placing the base with the workpiece beneath the inductor. A lid descends to prevent the axial movement of the workpiece during the process. To this set, we refer to it as a station. The inductor then moves vertically, contacting the workpiece and aligning itself with its center. This precise alignment is crucial to prevent uneven heating on either side of the crown, which could lead to variations in the hardened area thickness, besides minimizing the risk of accidents and equipment damage. At this point, the station with the workpiece starts rotation and heating for a predetermined duration. A water–polymer mixture is poured onto the crown upon reaching the heating time, ultimately hardening the product.

The use of polymer aims to achieve higher and more uniform cooling rates throughout the part compared to cooling with water alone. This mixture generates lower thermal and transformation gradients, reducing the likelihood of cracks and distortions compared to cooling in a vaporizable medium. The polymer utilized at the cooling stage is YUSHIRO QUENCHANT HSC at an 8% concentration. The part undergoes tempering at this stage, but the temperature is unsuitable for handling. Therefore, at the next position (before unloading), the part is cooled down to a temperature below 30 °C.

Five parts were selected before induction to evaluate the distortions induced by the hardening process. The central hole diameter of the parts served as the characteristic for assessment. Measurements were conducted using a MITUTOYO CRYSTA APEX S coordinate measuring machine, with the evaluation method including the measurement of 20 points and the calculation of the average diameter.

The process parameters used in the tests were as follows:

- Power: 93%;
- Warm-up time: 8 s;
- Shower flow rate: 35 L/min;
- Speed: 100 rpm.

The frequency and power have been regulated to ensure the part meets specifications (hardened region and hardness). The heating temperature is a consequence of the process parameters. Measurements show that the transmission crown reaches 1000 °C during induction, observed using a FLIR T440 thermographic camera with an emissivity of 0.85, as depicted in Figure 4.

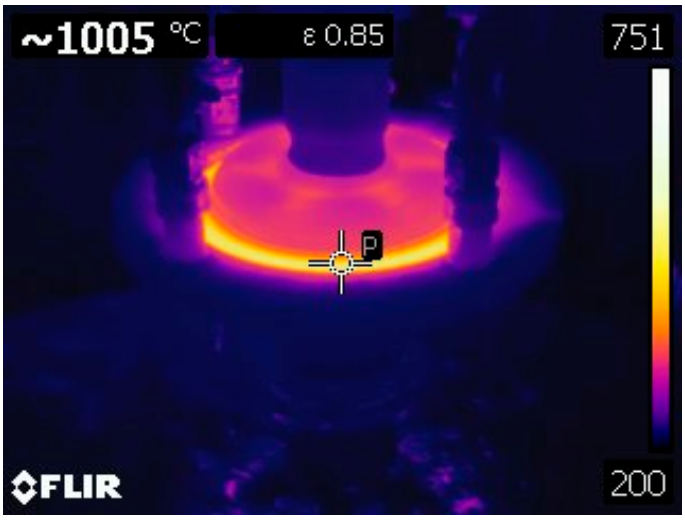

Figure 4. Temperature measurement of the transmission crown during heating.

This temperature guarantees phase transformation and fulfills product requirements. However, the heating and cooling cycle induces product deformation. Combined with variations from prior stamping and machining processes, this can compromise dimensional tolerances. Consequently, deformation studies were performed during the development of the new product to mitigate these issues.

2.2. Numerical Analysis—Computational

The numerical analysis was divided into two phases: thermal analysis and structural analysis, utilizing the experimental results of the hardening process. Initially, a 3D model of the transmission crown, fastening devices, base, and cover was developed using a CAD tool (Autodesk Inventor) 2022, as shown in Figure 5.

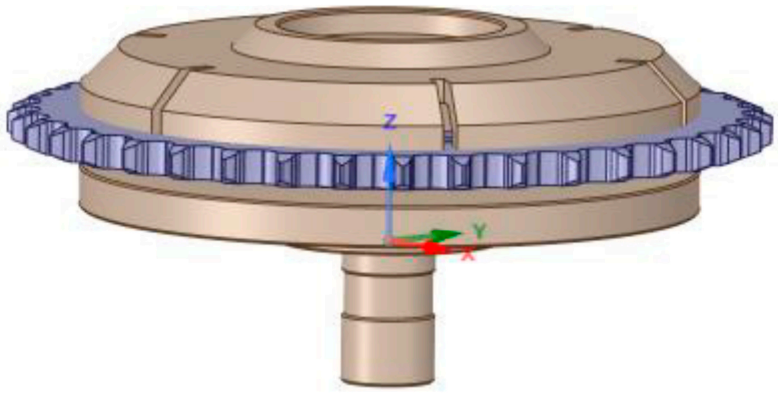

Figure 5. Three-dimensional model of the fastening system.

The 3D model is the basis for numerical analysis and is imported into Ansys Mechanical software 2022 R1. This enables a transient thermal study to evaluate the temperature gradient during heating. The second stage of numerical analysis involves structural analysis to assess the stresses in the crown at the end of the cycle. Finally, topological optimization is performed on the clamping devices to define a more suitable geometry. The objective is to obtain a base with reduced mass that minimizes its influence on the part's temperature distribution during heating, functioning solely as a process support. Figure 6 illustrates the flowchart of the numerical computational part, encompassing the stages of thermal analysis, structural analysis, optimization, and the case studies analyzed in this work using the Ansys platform.

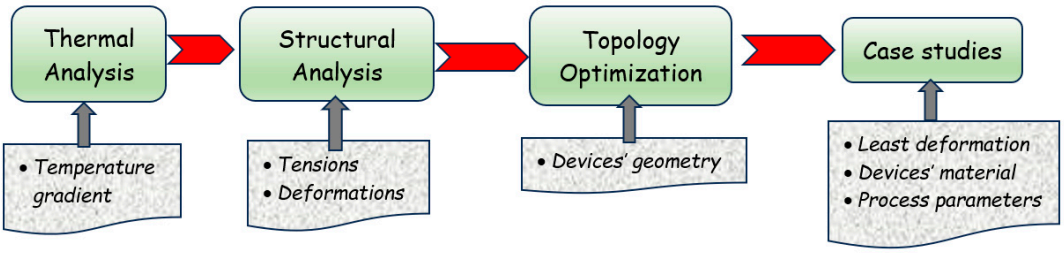

Figure 6. Flowchart of computational numerical modeling.

2.2.1. Material

The initial simulation stage entails material selection. The transmission crown material adheres to the SAE standard, which is 1045 carbon steel (Timóteo, MG, Brazil), while the fasteners, base, and cover are constructed from AISI 420 stainless steel (São Paulo, SP, Brazil), as detailed in Table 2.

Table 2. Properties of the materials.

Property	1045 Steel	AISI 420
Coefficient of thermal expansion ($°C^{-1}$)	1.15×10^{-5}	1.03×10^{-5}
Poisson	0.29	0.24
Shear stress (GPa)	80	80.87
Thermal conductivity	48.9 W/m·K at 25 °C	24.9 W/m·K at 25 °C
Specific heat	0.475 J/g·K at 25 °C	0.46 J/g·K at 25 °C
Electrical resistivity	0.0000171 Ω·m at 25 °C	0.000055 Ω·m at 25 °C

2.2.2. Mesh Construction and Evaluation

The mesh evaluation process involved analyses with diverse element sizes to assess the temperature response, as shown in Table 3. The objective was to evaluate the temperature response and calculation time to determine an appropriate mesh size, thereby reducing computational demands.

Table 3. Mesh element size tests.

Element Size [mm]	Nodes	Elements	Calculation Time [s]	Tmax
0.8	836,558	478,533	1041	351.8
1	543,853	309,357	610	350.98
1.5	265,145	147,562	265	348.38
2	169,352	92,986	187	407.16
3.5	113,961	61,490	145	488.43
4	95,822	51,566	116	489.49
5	77,208	40,918	92	479.12
10	50,109	25,885	60	466.22

Notably, within the range of 0.8–1.5 mm, the discrepancy in results among the different meshes was 3.42 °C. These temperature deviations are within an acceptable range, especially considering the substantial temperature fluctuation of 1100 °C during the heating and tempering. The 3.42 °C variance corresponds to a mere 0.29% error in the simulation, indicating a high level of accuracy. Consequently, a mesh size of 1.5 mm was chosen for the simulation and subsequent parametric studies. The mesh configuration selected for the computer simulation is illustrated in Figure 7.

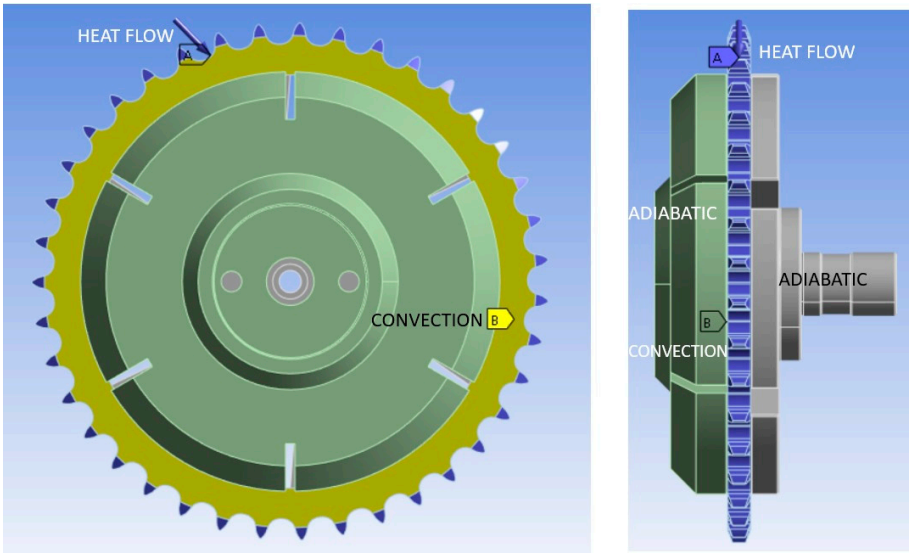

Figure 7. Selected mesh size 0.5 mm.

2.2.3. Boundary Conditions

Initially, the heat flow boundary condition is defined. The equipment has a nominal power of 125 kW. However, it is necessary to account for the losses in the equipment. Traditionally, the following efficiencies are used:

- Induction efficiency = 60%;
- Inductor loss = 2%.

The power transferred to the workpiece is calculated to be 73.5 kW. Given that only 93% of this power is effectively utilized in the defined process, the adjusted power value is 65 kW. Subsequently, convection is incorporated into the model. For convection, the value of the convection coefficient is unknown and needs to be estimated. The correlation utilized for this estimation is sourced from Incropera et al. [34]. The specific scenario under consideration involves a cylinder subjected to cross-flow, as described by Equation (1).

$$Nu_D = C * Re_D^m * Pr^{1/3} \quad (1)$$

For the Reynolds number, the following values were considered:

- Flow = 35 L/min;
- D = 2 mm (diameter of the water outlets);
- Specific mass = 1000 kg/m^3;
- Viscosity = 0.000907 Ns/m^2.

Some considerations must be made when calculating this coefficient: (a) the calculation does not consider the water boiling; and (b) the calculation does not consider the polymer mixture (8%). Consequently, the Reynolds number was calculated to be 17,050. For this specific Reynolds number, we obtained the constants C and m values for Equation (1), as presented in Table 4. The values of C and m were found to be 0.193 and 0.618, respectively, as shown in the table below. Figure 7 shows the boundary conditions used in the study.

Table 4. Constants of Equation (1). Adapted from Incropera et al. [34].

Reynolds	C	m
0.4–4	0.989	0.330
4–40	0.911	0.385
40–4000	0.683	0.466
4000–40,000	0.193	0.618
40,000–400,000	0.027	0.805

The calculated Nusselt number was 146.37; considering the thermal conductivity of k = 0.58 W/m-K for the transmission crown, the value of the convective coefficient was 8000 W/m^{2}K using Equation (2).

$$h = \frac{Nu \cdot k}{D} \quad (2)$$

3. Analysis and Discussion of Results

This section presents a comparison of the results and case analyses carried out, considering the following subsections:

- Comparison of computational and empirical findings from a thermal and structural perspective;
- Topological optimization outcomes;
- Case studies post-optimization.

3.1. Comparative Thermal Analysis

After conducting the simulation, the temperatures are calculated and graphed throughout the process, spanning from the initial heating phase to the completion of cooling. Figure 8 illustrates the outcomes within the transmission crown tooth region.

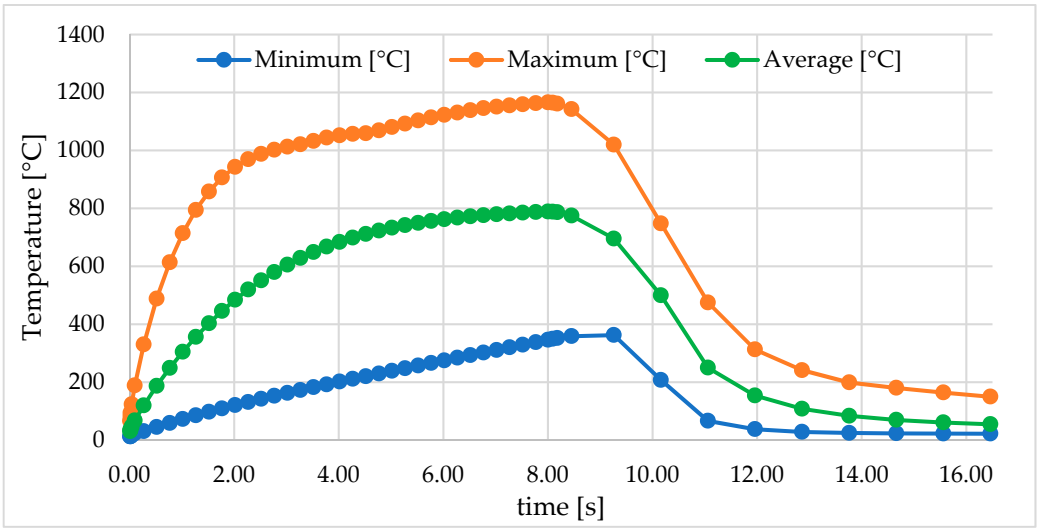

Figure 8. Temperature profile in the process.

It is noticeable that the maximum temperature at the end of the process closely aligns with the experimental findings. Following the process, the crown's maximum temperature reached 168 °C, as illustrated in Figure 9, exhibiting proximity to historical data. This investigation underscores the necessity of a dedicated cooling station post-induction. Such a station would facilitate the equipment operator's safe handling of the workpiece after adequate cooling.

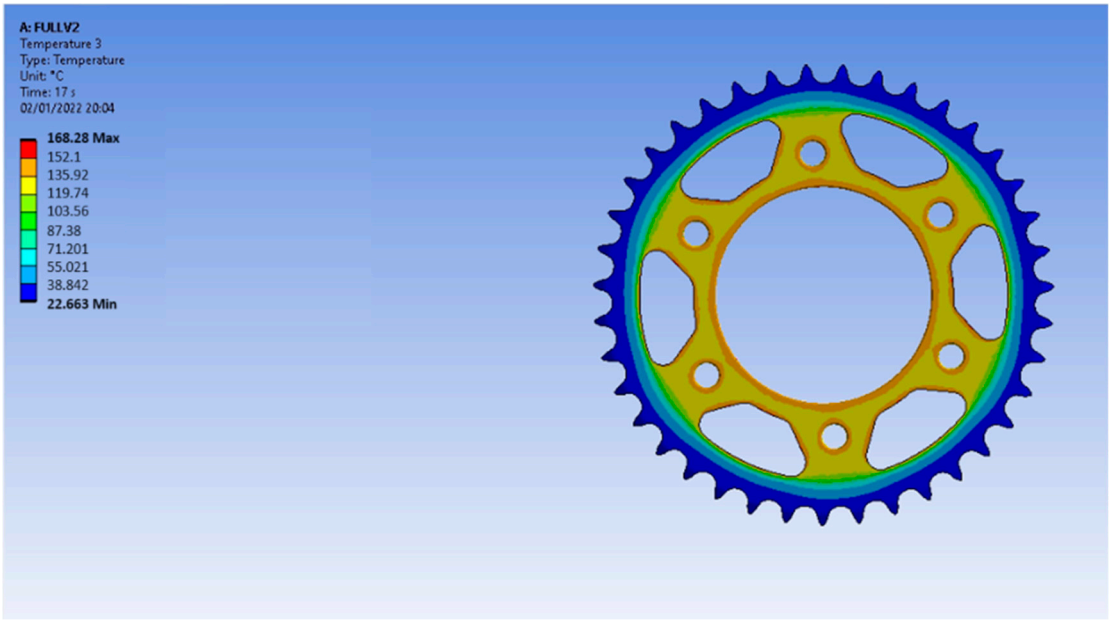

Figure 9. Temperature at the end of the process.

Table 5 compares the maximum temperatures obtained in the simulation and the experimental results.

Table 5. Comparison of temperatures.

	Maximum Temperature (°C)
Simulation	1166.5
Experiment	1239
Difference	72.5 (6.22%)

The difference may result from difficulty in measuring the temperature with the available instruments. The most considerable difficulty is regulating the emissivity depending on the material and positioning the instrument to measure the part. As it is mass production equipment, there is not much space for adequate and safe positioning of the instrumentation. In the case of the simulation step, it could influence parameter inputs in the model, such as material properties, convection coefficients, and the power reported by the equipment may not be exactly the real one due to the deficiency arising from the age of manufacture of the machine. The temperature difference certainly impacts the deformation value and the reliability of the parameters provided by the equipment, and the temperature measurement in the process would need to be investigated. Despite the differences, this value is relatively small due to the problems mentioned here and according to what is found in the literature with similar relative errors [21,22].

3.2. Comparative Deformation Analysis

A structural analysis is conducted following the thermal investigation to verify the distortion values. The outcome of this simulation is depicted in Figure 10. Five components were measured before and after induction. The values selected for comparison were the average deformations experienced by the product.

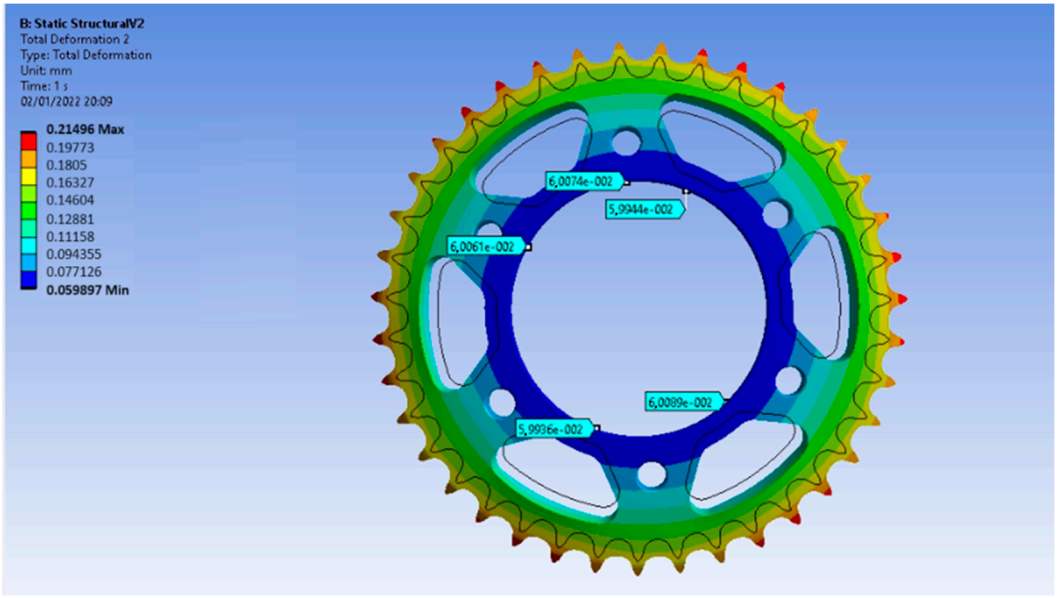

Figure 10. Deformation at the end of the process.

The adoption of an average value arises from the fact that the crown exhibits non-uniform deformation along the bore due to the diminutive thickness (7.2 mm) compared to the outer diameter (163 mm). This deformation induces ovalization in the crown hole. The study piece was measured with a coordinate measuring machine, measuring the hole at half thickness with twenty equidistant points along the hole and calculating the average distance of these points from the theoretical circle. As the part has shape errors resulting from the turning process, this greater number of points aims to minimize the effect of the circularity of the hole. As the 3D model does not present such variation, the average value of four equidistant points was evaluated. The measurements obtained from the coordinate measuring machine account for the number of points utilized to form the circle representing the hole and an average circle is calculated based on these points. When conducting this type of evaluation, the deviations of the points from the mean circle describe the shape error of the feature, known as ovalization (roundness).

The deformation values in the central hole were approximately 0.059 mm, which closely aligns with the experimental result of 0.063 mm. Notably, the 0.063 mm deformation value is an average, and some regions exceed and fall below this value. This variation stems from fluctuations in the composition of the raw material, the positioning of the workpiece in the device since it is a manual feed, gaps between the central guide and the workpiece, and variations in the measuring instruments and the equipment. Table 6 summarizes the deformation values found in the simulation compared to the value discovered experimentally.

Table 6. Comparative analysis of the deformations of the central bore (simulation x experiment).

	Deformation (mm)
Simulation	0.059
Experiment	0.063
Difference	0.004 (6.78%)

Although not the most significant deformation in the crown, the bore diameter holds paramount importance due to its critical tolerance. The deformation magnitude within the bore accounts for approximately 45% of the final product tolerance. In contrast, in other areas like the tooth region and stamped reliefs, this deformation only contributes to around

15% of the final tolerance. Consequently, this article primarily concentrates on the bore diameter deformation, given its substantial impact on the overall product quality.

3.3. Topological Optimization

Subsequently, topology optimization was conducted for the deformation assessment. For a holistic investigation of the heat distribution, the station is also considered part of the object for the simulations, although it will not undergo geometry optimization analysis. Initially, specific regions of the station were delineated and annotated to prevent their exclusion during the optimization process. These delineated regions hold significance as they are (precisely) the clamping and support mechanisms of the component within the equipment. The regions highlighted in red are set as imperatives to retain within the optimization process, as illustrated in Figure 11.

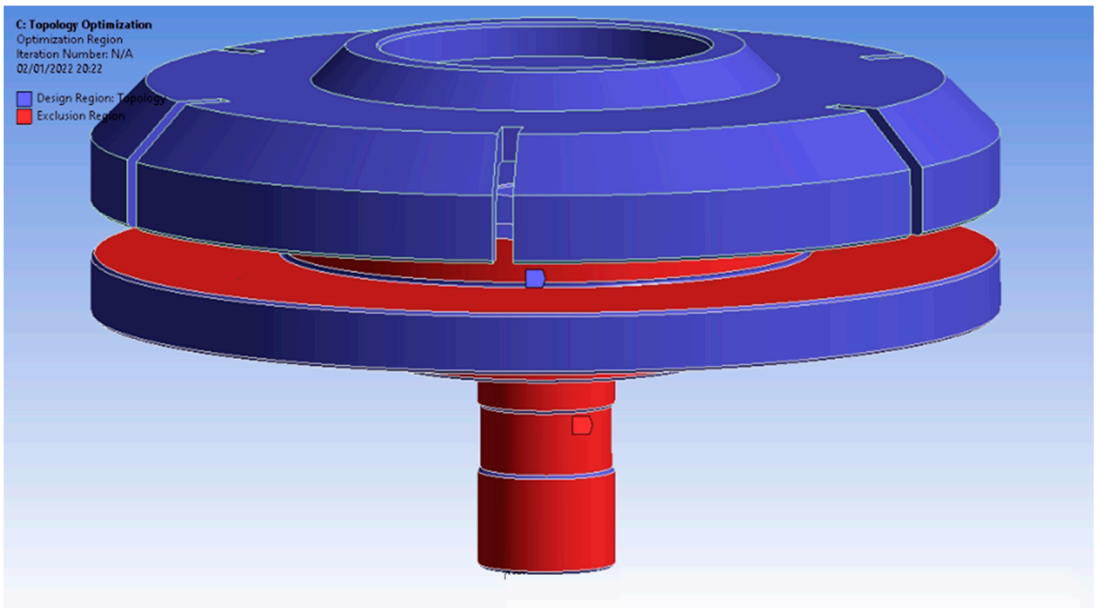

Figure 11. Regions to be included in the optimization.

As an objective, a 50% reduction in mass was targeted during the optimization process. The ANSYS software 2022 R1 was set to perform a maximum of five hundred iterations to calculate the material removal. The optimization outcome is depicted in Figure 12, which highlights the regions that should be preserved.

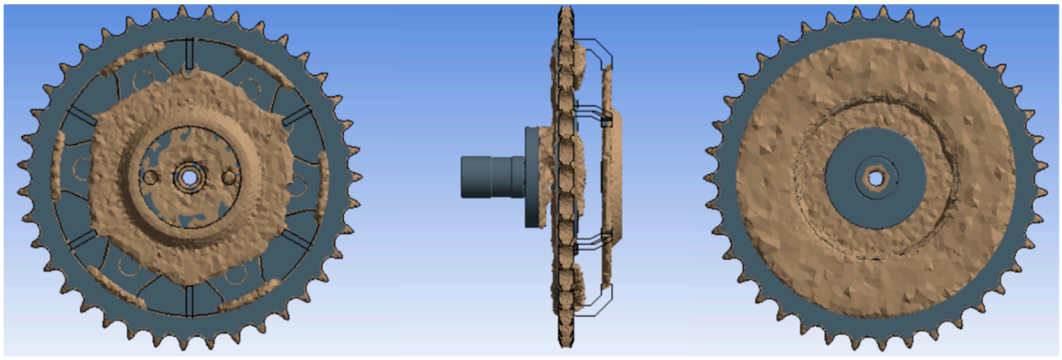

Figure 12. Topological optimization result of the fixture device.

The results demonstrate the areas of the geometry that can be removed without affecting the simulation. In Figure 12, the brown part is the material left after optimization, and the gray part is the optimized component material.

Examining the results, it is evident that, while the central part can be removed, this is not feasible in practice as it is integral to the system for attaching the base to the equipment. However, adjustments can be made to the base, reducing its weight. Additionally, the thickness of the base can be decreased. Reducing the mass of the support reduces the energy absorption capacity. It transmits more temperature to the crown and reduces the thermal inertia in the tempering process, and thus reducing the crown production time.

Before validating the new geometry, an assessment must be conducted to prevent warping or breakage during the process, ensuring the machine operator's safety.

The results indicate that the transmission crown geometry can be revised without impacting the deformation. The new geometry can be more cost-effective, as it consumes less material, allowing for cheaper and faster manufacturing processes. Reducing the cost of the devices directly impacts the manufacturing expenses

3.4. Sensitivity Analysis—Case Study

Case studies followed the validation process to examine the impact of parameters incorporated into the model. The first case focused on the material. Initially, stainless steel was utilized for the bases and lids. However, this material is costly, prompting an investigation into the feasibility of employing SAE 1045 steel. Concurrently, the study considered variations in the cooling water temperature, simulating the equipment's control system responding to changes in the ambient temperature. The equipment has a cooling system that maintains the water temperature within the range of 25 ± 2 °C.

Figure 13 presents the parameterized study and the influence of the material on the deformation at various water–polymer mixture temperatures. The results indicate that the deformations were remarkably similar, with a negligible difference of 0.001 mm, which falls within the acceptable level of deformation (a 1.6% difference).

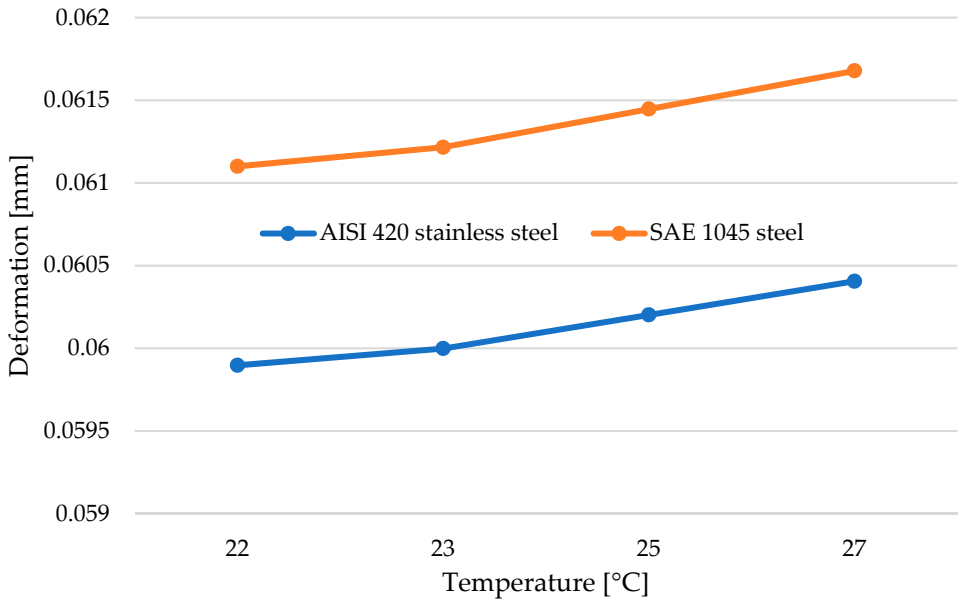

Figure 13. Influence of material on deformation at the central bore of the gear.

As a potential alternative, a new device could be designed and manufactured for testing purposes. By substituting stainless steel with carbon steel, the cost of raw materials for the base can be reduced by 40%. However, it is essential to consult with the equipment supplier to determine whether this material specification is based on any other issue not addressed by the simulation and not yet visible at this stage.

A new case study was conducted, this time incorporating variations in the heating power in addition to those explored in the previous case. Table 7 summarizes the results of this test. For the study, a power variation of ±5% was considered, and the range that

can be adjusted during the preparation process. These power variations are implemented to compensate for the variations in the part, such as those arising from the differences in raw material batches. The distortion results from present variations within the mechanical adjustment and dimensional tolerances that are very small, making the product unusable. All simulation and experimental data considered the sensitivity of parameters in the results.

Table 7. A general summary of the results of the cases studied. Influence of power (w), base material, and water temperature (°C) over piece deformation (mm) and temperature (°C).

Test No.	Power (W)	Base Material	Water Temperature (°C)	Maximum Deformation (mm)	Minimum Deformation (mm)	Maximum Temperature (°C)
1	65,000	AISI 420 stainless steel	22	0.214	0.059	1165
2	65,000	AISI 420 stainless steel	23	0.214	0.059	1166
3	65,000	AISI 420 stainless steel	25	0.214	0.060	1167
4	65,000	AISI 420 stainless steel	27	0.213	0.060	1167
5	65,000	SAE 1045 steel	22	0.252	0.061	1174
6	65,000	SAE 1045 steel	23	0.252	0.061	1175
7	65,000	SAE 1045 steel	25	0.251	0.061	1176
8	65,000	SAE 1045 steel	27	0.251	0.061	1176
9	61,750	AISI 420 stainless steel	22	0.204	0.056	1108
10	61,750	AISI 420 stainless steel	23	0.204	0.057	1109
11	61,750	AISI 420 stainless steel	25	0.203	0.057	1109
12	61,750	AISI 420 stainless steel	27	0.203	0.057	1110
13	61,750	SAE 1045 steel	22	0.239	0.058	1117
14	61,750	SAE 1045 steel	23	0.239	0.058	1117
15	61,750	SAE 1045 steel	25	0.239	0.058	1118
16	61,750	SAE 1045 steel	27	0.238	0.058	1119
17	68,250	AISI 420 stainless steel	22	0.225	0.062	1223
18	68,250	AISI 420 stainless steel	23	0.225	0.062	1223
19	68,250	AISI 420 stainless steel	25	0.225	0.063	1224
20	68,250	AISI 420 stainless steel	27	0.224	0.063	1225
21	68,250	SAE 1045 steel	22	0.265	0.064	1232
22	68,250	SAE 1045 steel	23	0.264	0.064	1232
23	68,250	SAE 1045 steel	25	0.264	0.064	1233
24	68,250	SAE 1045 steel	27	0.263	0.064	1234

This study demonstrates that a simultaneous increase in water temperature and power directly and significantly impacts deformation values, leading to an increase in these values. This increase in deformation (0.009 mm) specifically for that part does not have a substantial effect, as it does not necessitate a finishing process after heat treatment. However, it does result in increased electricity consumption, thereby making the process more costly.

Conversely, reducing power and water temperature values leads to a decrease in deformation values and lower electricity consumption. Nevertheless, these reduced values directly impact meeting hardness specifications and the depth of the hardened layer, as they alter the dynamics of the phase transformation. Experimental verification is essential to validate these new parameters.

3.5. Limitations and Futures Research Directions

This study attempted to fill the gap related to predicting structural deformation due to thermal induction and topology optimization in toothed gears by developing a computational procedure and validating processes in the automotive sector. For the simulation, the addition of the polymer was not taken into account, leaving the improvement of the model for future work. No literature was found that includes the effect of the polymer in the simulation. In physical experiments, the study of Hajék et al. [35], who evaluated the effects of induction quenching process parameters such as water temperature, polymer concentration in the water during quenching and rotation on the distortion of a cylinder, performing tests varying such parameters and TENSI et al. [36] compared the cooling gradients of a cylinder in a medium composed of water and polymer versus a vaporized medium (oil).

There are some limitations, including the following:

- ➢ Limitations regarding the Ansys® computational 2022 R1 model in capturing all the real complexities of the part due to geometry and material;
- ➢ Study based on the operating conditions of a single manufacturer in Brazil;
- ➢ Limitation in the generalization of results to other industrial applications;
- ➢ In the study, only the maximum temperature and average distortion in the central hole were considered without analyzing the temperature and distortion distribution in the gear teeth region.

Regarding possible future research directions related to the proposal:

- ✔ Analyze the use of alternative materials to increase the efficiency and cost–benefit ratio of the manufacturing process;
- ✔ Analyze other types of cylindrical gears within the scope of the induction hardening process;
- ✔ Optimize the computational model to improve the accuracy of deformations under thermal induction hardening conditions;
- ✔ Refine the topology optimization to identify removable regions without compromising the structural integrity of components;
- ✔ Machine learning techniques optimize the parameters of the induction hardening process, reducing the need for extensive and expensive experimental tests.

4. Conclusions

The present study aimed to analyze and optimize the thermal induction process applied to toothed crowns, focusing on thermal aspects, structural deformation, and topology optimization, as well as exploring the feasibility of different materials and operating conditions from a holistic point of view, considering some machinery structures (stations) as the subject of analysis. Among the key findings are the following:

- The comparative thermal analysis revealed that the maximum temperatures obtained in the computer model (1166 °C) closely aligned with the experimental results (1239 °C), with a maximum relative error of less than 6%. This indicates the reliabil-

ity and accuracy of the simulation model in predicting the thermal behavior of the induction process;

- The maximum temperature at the end of the process observed experimentally was 168 °C, underscoring the necessity of a cooling station to ensure the safe handling of the post-process part;
- In the deformation analysis, the simulated average deformations (0.059 mm) were also in agreement with the experimental results (0.063 mm), with a maximum relative error of less than 7%;
- Deformation in the central hole (bore) is critical due to the high precision required, representing 45% of the product's final tolerance. The accuracy obtained suggests that the simulation model is suitable for predicting and controlling deformations within acceptable limits.
- The topology optimization process identified areas of the part that can be removed without compromising structural and functional integrity. While some central parts cannot be removed due to their function in the fastening system, it is feasible to reduce the thickness and include reliefs in the base. These changes can result in lighter and less expensive devices without negatively impacting deformations, thereby optimizing manufacturing costs;
- The sensitivity analysis demonstrated that replacing AISI 420 stainless steel with SAE 1045 steel could significantly reduce material costs by up to 40%;
- Variations in heating power and cooling water temperature were analyzed, revealing that adjustments to these parameters can control deformation and energy consumption. A reduction in power and temperature can decrease deformation and energy consumption, although further tests are required to confirm compliance with the hardness and depth specifications of the hardened layer.
- Overall, the topology optimization and sensitivity study suggest several opportunities to reduce the costs and improve the process efficiency. This study contributes to a better understanding and control of the thermal induction process, enabling advancements in manufacturing toothed transmission crowns with greater precision and lower cost.

Author Contributions: Conceptualization, P.M.P., J.Â.P.d.C. and L.A.P.G.; methodology, P.M.P., J.Â.P.d.C. and L.A.P.G.; software, P.M.P. and J.Â.P.d.C.; validation, P.M.P., J.Â.P.d.C. and L.A.P.G.; formal analysis, P.M.P.; investigation, P.M.P.; resources, P.M.P., J.Â.P.d.C., A.A.V.O., L.A.P.G. and G.d.N.P.L.; data curation, P.M.P. and J.U.J.; writing—original draft preparation, P.M.P., J.U.J., P.S.A.M., K.G.B.A. and A.A.V.O.; writing—review and editing, J.Â.P.d.C., G.d.N.P.L., K.G.B.A. and A.A.V.O.; visualization, P.M.P. and L.A.P.G.; supervision, J.Â.P.d.C., L.A.P.G., A.A.V.O. and P.S.A.M.; project administration, J.Â.P.d.C., L.A.P.G., A.A.V.O., J.U.J. and P.S.A.M.; funding acquisition, J.Â.P.d.C., G.d.N.P.L., A.A.V.O. and K.G.B.A. All authors have read and agreed to the published version of the manuscript.

Funding: This research received no external funding.

Data Availability Statement: The data should be share as resquested. Some data are confidential.

Acknowledgments: The authors thank the PPGEM/UFPE and Capes for supporting the master's dissertation. The fourth, fifth, and seventh authors thank the IFPE and CNPq for their support (IFPE/2023, 3303417/2022-6, 303200/2023-5), respectively.

Conflicts of Interest: The authors declare no conflicts of interest.

References

1. Zhi, S.; Wu, H.; Shen, H.; Wang, T.; Fu, H. Entropy-Aided Meshing-Order Modulation Analysis for Wind Turbine Planetary Gear Weak Fault Detection under Variable Rotational Speed. *Entropy* **2024**, *26*, 409. [CrossRef] [PubMed]
2. Li, J.; Cui, Q.; Pang, C.; Xu, P.; Luo, W.; Li, J. Integrated vehicle chassis fabricated by wire and arc additive manufacturing: Structure generation, printing radian optimisation, and performance prediction. *Virtual Phys. Prototyp.* **2024**, *19*, e2301483. [CrossRef]
3. Liu, H.; Zhao, J.; Tang, J.; Shao, W.; Sun, B. Simulation and Experimental Verification of Die Quenching Deformation of Aviation Carburized Face Gear. *Materials* **2023**, *16*, 690. [CrossRef] [PubMed]

4. Chaubey, S.K.; Jain, N.K. State-of-art review of past research on manufacturing of meso and micro cylindrical gears. *Precis. Eng.* **2018**, *51*, 702–728. [CrossRef]
5. Ildefonso, B.; Storer, D. State-of-the-art Analysis on Alternative Materials for the Automotive Industry. *Transp. Res. Procedia* **2023**, *72*, 1560–1567. [CrossRef]
6. Boral, P.; Gołębski, R.; Kralikova, R. Technological Aspects of Manufacturing and Control of Gears—Review. *Materials* **2023**, *16*, 7453. [CrossRef]
7. Yumak, N.; Aslantas, K. A review on heat treatment efficiency in metastable b titanium alloys: The role of treatment process and parameters. *J. Mater. Res. Technol.* **2020**, *9*, 15360–16280. [CrossRef]
8. Tong, D.; Gu, J.; Yang, F. Numerical simulation on induction heat treatment process of a shaft part: Involving induction hardening and tempering. *J. Mater. Process. Technol.* **2018**, *262*, 277–289. [CrossRef]
9. Almeida, D.I.S.d.; Arrais, D.F.; Leitão, M.J.M. Influencia Dos Diferentes Tratamentos Termicos Na Microestrutura Do Aço Sae 8620. In Proceedings of the Anais do Enemt—Encontro Nacional de Estudantes de Engenharia Metalúrgica, de Materiais e de Minastalúrgica, de Materiais e de Minas, São Paulo, Spain, 2–6 October 2017; Volume 17, pp. 111–121. [CrossRef]
10. Abdallah, M.; Azevedo-Scudeller, L.; Hiolle, M.; Lesur, C.; Baniel, A.; Delaplace, G. Review on mechanisms leading to fouling and stability issues related to heat treatment of casein-based RTD beverages. *Food Bioprod. Process.* **2022**, *136*, 67–83. [CrossRef]
11. Asadzadeh, M.Z.; Raninger, P.; Prevedel, P.; Ecker, W.; Mücke, M. Hybrid modeling of induction hardening processes. *Appl. Eng. Sci.* **2021**, *5*, 100030. [CrossRef]
12. Kim, D.W.; Cho, H.H.; Lee, W.B.; Cho, K.T.; Cho, Y.G.; Kim, S.J.; Han, H.N. A finite element simulation for carburizing heat treatment of automotive gear ring incorporating transformation plasticity. *Mater. Des.* **2016**, *99*, 243–253. [CrossRef]
13. Park, S.; Kim, D.W.; Kim, J.H.; Lee, S.Y.; Kwon, D.; Han, H.N. A finite element simulation for induction heat treatment of automotive drive shaft. *ISIJ Int.* **2020**, *60*, 1333–1341. [CrossRef]
14. Rattanaudompisut, A.; Charoenwiangnuea, P. Experimental study on induction heating generation for plastic deformation. *Mater. Today Proc.* **2023**. [CrossRef]
15. Sun, B.; Liu, H.; Tang, J.; Rong, S.; Liu, Y.; Jiang, W. Optimization of heat treatment deformation control process parameters for face-hobbed hypoid gear using FEA-PSO-BP method. *J. Manuf. Process.* **2024**, *117*, 40–58. [CrossRef]
16. Vieweg, A.; Ressel, G.; Prevedel, P.; Raninger, P.; Panzenböck, M.; Marsoner, S.; Ebner, R. Induction hardening: Differences to a conventional heat treatment process and optimization of its parameters. *IOP Conf. Ser. Mater. Sci. Eng.* **2016**, *119*, 012019. [CrossRef]
17. Tyflopoulos, E.; Lien, M.; Steinert, M. Optimization of brake calipers using topology optimization for additive manufacturing. *Appl. Sci.* **2021**, *11*, 1437. [CrossRef]
18. Borda, F.; La Rosa, A.D.; Filice, L.; Gagliardi, F. Environmental impact of process constrained topology optimization design on automotive component' life. *Int. J. Mater. Form.* **2023**, *16*, 48. [CrossRef]
19. Lee, K.; Park, S.; Lee, Y.; Kim, J.; Kim, S.H. New concept carrier of front-end module with structural topology optimization for automotive. *Adv. Mech. Eng.* **2022**, *14*, 1–9. [CrossRef]
20. Armentani, E.; Giannella, V.; Parente, A.; Pirelli, M. Design for NVH: Topology optimization of an engine bracket support. *Procedia Struct. Integr.* **2020**, *26*, 211–218. [CrossRef]
21. Huang, B.; Zhang, H.; Ding, Y. CFD Modelling and Numerical Simulation of the Windage Characteristics of a High-Speed Gearbox Based on Negative Pressure Regulation. *Processes* **2023**, *11*, 804. [CrossRef]
22. Mitov, A.; Nikolov, N.; Nedelchev, K.; Kralov, I. CFD Modeling and Experimental Validation of the Flow Processes of an External Gear Pump. *Processes* **2024**, *12*, 261. [CrossRef]
23. Dziatkiewicz, G.; Kuska, K.; Popiel, R. Evolutionary Optimizing Process Parameters in the Induction Hardening of Rack Bar by Response Surface Methodology and Desirability Function Approach under Industrial Conditions. *Materials* **2023**, *16*, 5791. [CrossRef] [PubMed]
24. Garois, S.; Daoud, M.; Chinesta, F. Data-Driven Inverse Problem for Optimizing the Induction Hardening Process of C45 Spur-Gear. *Metals* **2023**, *13*, 997. [CrossRef]
25. Saputro, I.E.; Chen, C.P.; Jheng, Y.S.; Huang, H.C.; Fuh, Y.K. Mobile Induction Heat Treatment of Large-Sized Spur Gear—The Effect of Scanning Speed and Air Gap on the Uniformity of Hardened Depth and Mechanical Properties. *Steel Res. Int.* **2023**, *94*, 2200261. [CrossRef]
26. Jan, J.; MacKenzie, D.S. On the Development of Computational Fluid Dynamics Quenching Simulation Methodology for Effective Thermal Residual Stress Control. *J. Mater. Eng. Perform.* **2024**, *33*, 3986–4010. [CrossRef]
27. Areitioaurtena, M.; Segurajauregi, U.; Urresti, I.; Fisk, M.; Ukar, E. Predicting the induction hardened case in 42CrMo4 cylinders. *Procedia CIRP* **2020**, *87*, 545–550. [CrossRef]
28. Min, J.; Zhu, G.; Yuan, Y.; Liu, J. COMSOL Simulation for Design of Induction Heating System in VULCAN Facility. *Sci. Technol. Nucl. Install.* **2021**, *2021*, 9922503. [CrossRef]
29. Leitner, M.; Aigner, R.; Grün, F. Numerical fatigue analysis of induction-hardened and mechanically post-treated steel components. *Machines* **2019**, *7*, 1. [CrossRef]
30. Barglik, J.; Smagór, A.; Smalcerz, A.; Desisa, D.G. Induction heating of gear wheels in consecutive contour hardening process. *Energies* **2021**, *14*, 3885. [CrossRef]

31. Holmberg, J.; Hammersberg, P.; Lundin, P.; Olavison, J. Predictive Modeling of Induction-Hardened Depth Based on the Barkhausen Noise Signal. *Micromachines* **2023**, *14*, 97. [CrossRef]
32. Stević, Z.; Dimitrijević, S.P.; Stević, M.; Stolić, P.; Petrović, S.J.; Radivojević, M.; Radovanović, I. The Design of a System for the Induction Hardening of Steels Using Simulation Parameters. *Appl. Sci.* **2023**, *13*, 11432. [CrossRef]
33. Correa, M.L.R.; Schneider, E.L.; Tassoni, D.d.S.M.; Oliveira, R.M.; Dias, M.d.N.; Oliveira, C.T. A influência de diferentes taxas de resfriamento de polímero PAG nas distorções em peças de aço SAE 1050 no tratamento térmico de têmpera por indução The influence of different PAG polymer cooling rates on distortions in SAE 1050 steel parts on induction. *Technol. Metal. Mater. Mineração* **2023**, *20*, 1–9. [CrossRef]
34. Incropera, F.P.; DeWitt, D.P.; Bergman, T.L.; Lavine, A.S. *Fundamentals of Heat and Mass Transfer*, 6th ed.; John Wiley & Sons: Hoboken, NJ, USA, 2007.
35. Hájek, J.; Rot, D.; Jiřinec, J. Distortion in induction-hardened cylindrical part. In *Defect and Diffusion Forum*; Trans Tech Publications Ltd.: Stafa-Zurich, Switzerland, 2019; Volume 395, pp. 30–44. [CrossRef]
36. Tensi, H.M.; Canale, L.C.F.; Totten, G.E. The quenching process: An overview of the fundamental physics properties of liquid quenching. In Proceedings of the Congresso Anual da ABM, Rio de Janeiro, Spain, 21–24 July 2003; Volume 3, pp. 359–370.